Intense dust and extremely fresh biomass burning outbreak in Barcelona, Spain: Characterization of their optical properties and estimation of their direct radiative forcing

M. Sicard, M. Mallet, D. Garcia-Vizcaino, A. Comeŕon, F. Rocadenbosch, P. Dubuisson, C. Muñoz-Porcar

ENVIRONMENTAL RESEARCH
LETTERS

LETTER • OPEN ACCESS

Intense dust and extremely fresh biomass burning outbreak in Barcelona, Spain: characterization of their optical properties and estimation of their direct radiative forcing

To cite this article: M Sicard *et al* 2012 *Environ. Res. Lett.* **7** 034016

OPEN ACCESS
IOP PUBLISHING
ENVIRONMENTAL RESEARCH LETTERS
Environ. Res. Lett. **7** (2012) 034016 (6pp)
doi:10.1088/1748-9326/7/3/034016

Intense dust and extremely fresh biomass burning outbreak in Barcelona, Spain: characterization of their optical properties and estimation of their direct radiative forcing

M Sicard[1], M Mallet[2], D García-Vizcaíno[1], A Comerón[1], F Rocadenbosch[1], P Dubuisson[3] and C Muñoz-Porcar[1]

[1] RSLab/IEEC-CRAE, Universitat Politècnica de Catalunya, Barcelona, Spain
[2] Laboratoire d'Aérologie, Université de Toulouse/CNRS, Toulouse, France
[3] Laboratoire d'Optique Atmosphérique, Université de Lille 1, Lille, France

E-mail: msicard@tsc.upc.edu

Received 6 July 2012
Accepted for publication 31 July 2012
Published 24 August 2012
Online at stacks.iop.org/ERL/7/034016

Abstract
An extremely fresh smoke plume (<5 h) was transported over Barcelona on 23 July 2009, just 5 h after an intense Saharan dust event finalized. Both events were observed by sun-photometer, lidar and satellite systems. Results indicate surprisingly large absorption of mixed dust particles (SSA $\sim 0.83 \pm 0.04$) with lower SSA than that observed for smoke (0.86 ± 0.04) particles at 440 nm. Our investigation shows that dust particles may have mixed during their transport with anthropogenic and smoke particles. Dust and smoke layers are observed between 1–6 and 1–4 km, with associated lidar ratios at 532 nm of 51 and 36 sr, respectively. Due to low SSAs and moderate surface albedos, shortwave (SW) radiative forcing calculations reveal that a large part of the solar energy losses at the surface is gained by the atmosphere for each aerosol. Here, dust particles produced a positive instantaneous forcing at TOA (+8 W m^{-2} at 12 UT), while the smoke produced a negative forcing of −13 W m^{-2} at 17 UT. The associated SW heating rate is calculated to be around 2–3 K day^{-1} for both dust and smoke aerosols.

Keywords: fresh biomass burning, dust, lidar, direct radiative forcing

1. Introduction

In summer, the biomass burning aerosols affecting the Mediterranean region are mostly local due to the warm and dry Mediterranean climate which favors the ignition and the expansion of fires. These aerosols are able to significantly affect the regional climate as they influence directly the radiative budget (Formenti *et al* 2002). Biomass burning climatological studies around the Mediterranean are usually based on fresh (generally >24 h) (Alados-Arboledas *et al* 2011) and mostly on aged smoke particles (Formenti *et al* 2002). Very little literature is available for very fresh biomass burning (<24 h) despite its strong absorption characteristics due to its high content of soot. Additional observations of their

Table 1. Major optical properties of the plumes observed. The lidar ratio is the one obtained by applying the AOT-constrained inversion algorithm.

	22 July	23 July	24 July	
Lidar start time (duration)	1212 (30 min)	1719 (30 min)	0134 (150 min)	1219 (150 min)
AOT at 532 nm	0.59	0.41	0.11	0.13
AOT_{PBL} ($\frac{AOT_{PBL}}{AOT}$ in %)	0.10 (17%)	0.09 (22%)	0.05 (45%)	0.12 (92%)
LR at 532 nm (sr)	51	36	—	40
LR at 1064 nm (sr)	47	20	—	19

optical and microphysical properties as well as their altitude of transport are clearly needed to improve regional climate models. Such observations also present a real interest as most climate models project an increase in annual temperatures and drier summer conditions (Giorgi and Lionello 2008) that would increase the risk of fires over the Mediterranean. In the past 25 years, the total number of reported fires has risen sharply from ∼20 000 to 60 000 yr^{-1} in the five Mediterranean Member States of the EU15, France, Greece, Italy, Portugal and Spain (EEA 2006).

An event of very fresh biomass burning was captured in Barcelona, Spain, where the smoke was observed less than 5 h after it was emitted. It coincides with the end of an intense dust outbreak less than 5 h before. Here, we took advantage of those aerosol events to present a detailed characterization of the two types of aerosols and an estimation of their shortwave (SW) direct radiative forcing. An estimation of the SW heating rate due to both aerosols is also provided.

2. Instrumentation, tools and meteorological conditions

A CIMEL sun–sky photometer, part of the Aerosol Robotic Network (AERONET) and located in Barcelona in a urban area (41.38N, 2.11E, 125 m asl), was used to provide the following parameters for the whole atmospheric column in the spectral bands of 440, 675, 870 and 1020 nm: AOT, the aerosol optical thickness; AE, the Ångström exponent; SSA, the single scattering albedo; $dV(r)/d\ln r(r)$, the aerosol size distribution at a radius r; and SA, the surface albedo.

Taking into account all the information about the instrument precision, calibration precision and data accuracy (Holben *et al* 1998), the estimated accuracy of the AOT measurements is about ±0.02 for the level 2 data (cloud-screened and quality-assured) which are used in this letter. Dubovik *et al* (2002) reported an uncertainty of about 0.04 on SSA.

A Kipp and Zonen CM-21 pyranometer collocated to the sun-photometer and part of the Solar Radiation Network (SolRad-Net) network measured the total solar spectrum in the band 305–2800 nm, which after integration gives $L_{\downarrow}$, the solar downward flux at the surface.

The EARLINET lidar from the Universitat Politècnica de Catalunya is situated 600 m away from both passive instruments. The system employs a Nd:YAG laser at 532 and 1064 nm emitting equal pulses of 160 mJ energy at a repetition rate of 20 Hz. In reception the backscattered elastic radiation, and also the nitrogen Raman-shifted backscattered radiation at 607 nm, are recorded. During daytime, the aerosol optical coefficient profiles (backscatter and extinction) were retrieved by means of the two-component elastic lidar inversion algorithm (Fernald 1984, Sasano and Nakane 1984, Klett 1985) constrained with the sun-photometer-derived AOT. At nighttime the Raman lidar inversion algorithm was used (Ansmann *et al* 1990). The retrieval of the planetary boundary layer (PBL) height was made using the gradient method.

Satellite imagery such as MODIS and MSG/SEVIRI sensors were used to visualize the geographical distribution of the aerosol plumes observed from the ground. Ancillary tools such as Hysplit and DREAM models were also used to confirm the plumes' origin and trajectory.

The measurements presented in this letter were performed on 22 (J22), 23 (J23) and 24 (J24) July 2009, in the framework of the DAURE (Determination of the sources of atmospheric Aerosols in Urban and Rural Environments in Spain) campaign (Jorba *et al* 2011). From 20 to 23 July a deep low crossed Ireland then the United Kingdom, and moved forward with a cold front extending southward and affecting the Iberian Peninsula (IP). No precipitation was measured over northeastern Spain. At the same time, a strong anticyclonic circulation developed over central Algeria. The resultant southwest winds advected dust loads towards the southern IP which reached northeastern Spain on 21 July in the morning and lasted until 23 July.

3. Aerosol characterization

A summary of the lidar measurements performed during J22–J24 is presented in table 1. Figure 1 shows Hysplit back-trajectories arriving in Barcelona at the lidar measurement time in the PBL and in two more layers above it. Figure 1 also shows the total AOT at 500 nm, the fine and coarse mode AOT and the Ångström exponent calculated between 440 and 870 nm. Time series of the range-square-corrected signals (RSCS), extinction coefficient profiles and extinction-related Ångström exponents, AE^{α}, calculated between 532 and 1064 nm are also plotted in figure 1.

The AOT on J22 is high, between 0.54 and 0.77, and the coarse mode predominates (fine mode fraction ∼20%). The associated AE is quite low and oscillates around 0.2–0.5. At 1212 UT the PBL is below 1 km and the AOT trapped into it represents less than 20% of the total AOT. Aerosols are present above the PBL up to almost 6.0 km. The backtrajectories at 1.5 and 4.0 km are clearly coming from central Algeria and southern Morocco, respectively. The

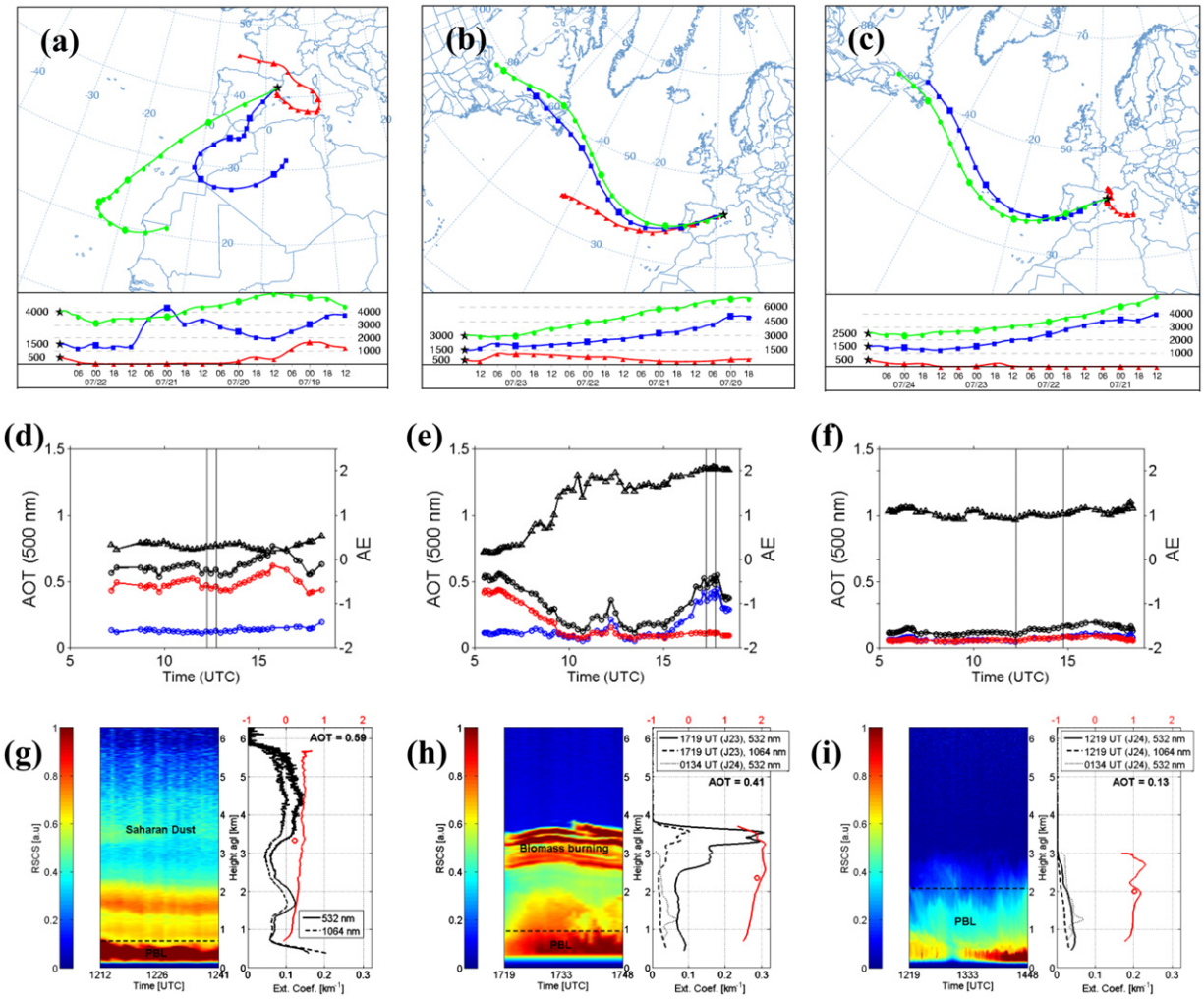

Figure 1. Back-trajectories arriving in Barcelona (a) on J22 at 12 UT, (b) on J23 at 17 UT and (c) on J24 on 12 UT. Total AOT at 500 nm (black circles), fine (blue circles) and coarse (red circles) mode AOT and Ångström exponent (black triangles, right axis) (d) on J22, (e) on J23 and (f) on J24. Lidar RSCS time series and extinction coefficient profiles (g) on J22, (h) on J23 and (i) on J24. In the plot of the extinction coefficient, the lidar-derived AE^{α} is reported in red (top axis) and the sun-photometer-derived AE averaged over the lidar measurement duration is represented by a red circle. In the last two plots the Raman-inverted extinction profiles of the J24 nighttime measurement has been added.

lidar-derived AE^{α} (figure 1(g)) is around 0.15 at 1 km and oscillates between 0.4 and 0.5 in the upper layer. The poor wavelength-dependency is also shown by the LR at 532 and 1064 nm which are nearly equals (51 and 47 sr, respectively). Those observations (predominance of the coarse mode, low Ångström exponents, LR $\sim$ 50 sr) are the signature of mineral dust.

On J23 the AOT drops from the early morning until 11 UT down to a seasonal mean value of 0.10–0.15 (Sicard *et al* 2011). At the same time the AE increases up to high values between 1.5 and 1.9 while the fine and the coarse mode reach equality. Around 15 UT the AOT starts to increase along with the fine mode while the AE also increases and stabilizes around 2.0. Figure 2 shows two images of MODIS taken on J23 at 1105 and at 1250 UT which clearly show the plume of a wildfire located 250 km southwest of Barcelona and transported in the direction of the city. All back-trajectories of figure 1(b), are coming from a southwest direction. Van Drooge *et al* (2012) showed by overlapping MODIS images and Hysplit back-trajectories that the transport of the plume from the source to Barcelona took approximately 5 h. We estimate that the fire started between 09 and 10 UT. At the time of the lidar measurement (1719 UT) the AOT is 0.41, the AE is 2.05 and the fine mode fraction is 80%. The PBL is around 1.0 km and the AOT trapped into it represents around 20% of the total AOT. Here, smoke aerosols are present above the PBL up to almost 4.0 km. The lidar time series and the extinction profile (figure 1(h)) captured very well the smoke plume between 2.5 and 4.0 km where strong extinction values up to 0.3 km^{-1} are observed. The lidar-derived AE^{α} in the smoke plume is around 2.0 and the lidar ratio is 36 sr at 532 nm. The backscatter color ratio (not shown) varies between 1.7 and 2.5 in the smoke plume, so that together with the value of lidar ratio found at 532 nm it fits very well in the classification of fresh smoke based on aerosol intensive variables made by Burton *et al* (2012). At 0134 UT on J24 the PBL is around 1.3 km (not shown). A residual layer of smoke might be present above it and up to almost 3 km. The

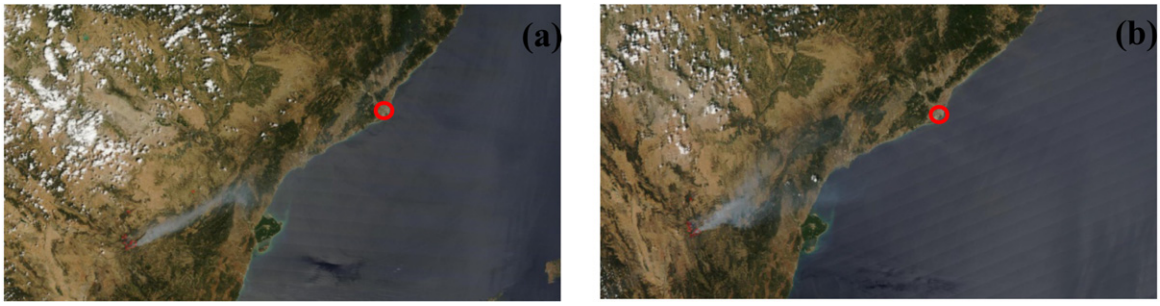

Figure 2. MODIS image taken on J23 (a) at 1105 UT and (b) at 1250 UT. The red circles indicate Barcelona.

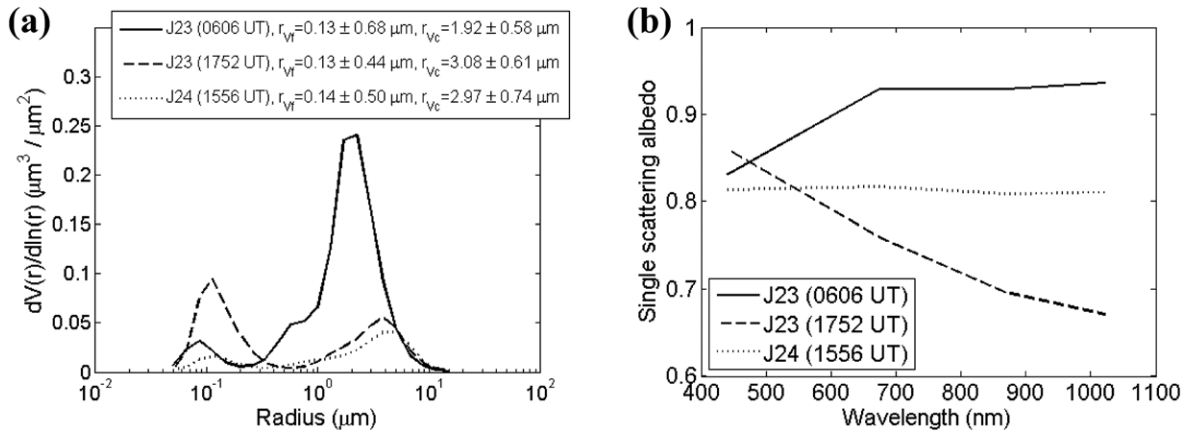

Figure 3. AERONET (level 2) columnar (a) volume size distribution and (b) single scattering albedo on J23 (at 0606 UT), on J23 (at 1752 UT) and on J24 (at 1556 UT). The volume median radius for the fine, r_{Vf}, and the coarse mode, r_{Vc}, and their associated standard deviation are reported in (a).

Raman-inverted LR in the layer above 2.0 km varies between 30 and 40 sr. This result agrees very well with the LR found on J23 which indicates the presence of smoke particles above the PBL.

On J24 the AOT has come back to a seasonal value varying between 0.09 and 0.2. The associated AE oscillates around 1.0, which is slightly above the seasonal value (Sicard *et al* 2011). At 1219 UT the PBL is developed up to 2.0 km. The mean AOT and AE are 0.13 and 1.0, respectively. The lidar-derived AE^{α} oscillates also around 1.0 in the PBL. The LR is 40 sr at 532 nm. For that day, the back-trajectory arriving in Barcelona at 500 m shows a local recirculation pattern. The backscatter color ratio is around 1.0 or slightly lower than 1.0. Those observations and the classification made by Burton *et al* (2012) suggest that the mixture observed no longer contains smoke but rather a mixing of maritime and polluted-maritime aerosols.

The day-by-day comparison of the columnar volume size distribution and SSA (figure 3) also evidences the different aerosol plumes observed. On the morning of J22, cirrus clouds were present and prevented the AERONET algorithm from producing level 2 data. We have selected the first level 2 data of J23 at 0606 UT to be representative of the situation on J22 since dust is still present and the columnar AOT and AE are similar to the values of J22. Figure 3(a) shows clearly the predominance of medium-size particles on J22 (i.e. observed on J23 at 0606 UT) and the predominance of rather small particles on J23. On J22 r_{Vc} (1.92±0.58) is in good agreement with the climatology established by Dubovik *et al* (2002). On J23 r_{Vf} (0.13 ± 0.44) is in the lower range of the same climatology, probably because the plume observed is very young (<5 h).

According to figure 3(b), a surprising and interesting result concerns the low mean value of the SSA derived on J22 (0.83 ± 0.04 at 440 nm), which is even lower than the smoke SSA mean value (at 440 nm only), indicating highly absorbing dust aerosols. We note that the observed dust size distribution is similar to that of the climatology established by Dubovik *et al* (2002) for desert dust in which they found an SSA of 0.92 ± 0.03 at 440 nm, in contrast to the imaginary part of the dust refractive index (0.010 ± 0.005 at 440 nm observed from AERONET), which is approximately four times larger than that reported in the same climatology. This result should contribute to reduce significantly the SSA and could be due to the possible mixing of dust with anthropogenic particles. This assumption is reinforced by the CALIPSO aerosol subtyping observations derived around 0145 UT on J23 (in an orbit a few hundreds of kilometers east of Barcelona), which clearly shows an aerosol plume up to 6 km composed of mixed dust, polluted dust and smoke particles. In addition, on MODIS Rapid Response Images many fires are clearly visible over northern Algeria. In that sense the low dust SSA might be due to a mixing of dust with polluted and smoke aerosols. This hypothesis should obviously now be associated with regional modeling exercises to make a definitive conclusion.

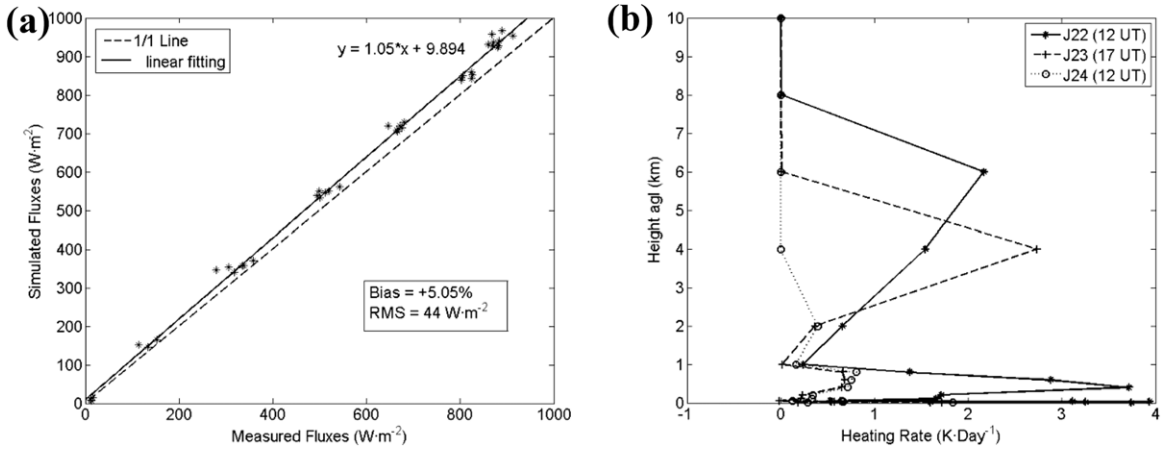

Figure 4. (a) Comparison of the simulated surface downward fluxes with the measured fluxes. (b) Profiles of instantaneous aerosol SW heating rates.

On J23 SSA is decreasing with wavelengths like in Dubovik *et al* (2002), Formenti *et al* (2002) or Cachorro *et al* (2008) who measured SSA of 0.91–0.94, 0.91 and 0.88 at 440 nm, respectively. The nature of the 'quasi-pure', fresh smoke observed in our study probably explains the rather low SSA found (0.86 ± 0.04 at 440 nm) that other authors such as Meloni *et al* (2006) also reported (0.80) for relatively fresh biomass burning.

Table 2. Instantaneous SW direct radiative forcing calculations at BOA, TOA and ATM on J22, J23 and J24.

	22 July at 12 UT	23 July at 17 UT	24 July at 12 UT
BOA (W m^{-2})	−93	−73	−17
TOA (W m^{-2})	8	−13	1
ATM (W m^{-2})	101	60	18

4. Direct SW radiative forcing calculations

The SW direct radiative forcing at bottom of atmosphere (BOA), at top of atmosphere (TOA), and into the atmospheric layer (ATM) were computed using the radiative transfer model GAME (Dubuisson *et al* 1996), which accounts for the scattering and absorption processes by particles and gases. In this model, the absorption includes the absorbers in the shortwave region. The methodology used in this work is detailed in Mallet *et al* (2008). Upward and downward net radiative fluxes F are computed over the spectral solar range 0.3–2.8 μm in 18 levels of the atmosphere between 0.005 and 20 km. From these fluxes, the direct forcings at the BOA, ΔF_{BOA}, and at the TOA, ΔF_{TOA}, are defined by:

$$\Delta F_{\mathrm{BOA}} = F^{\mathrm{w}}_{\mathrm{BOA}} - F^{\mathrm{o}}_{\mathrm{BOA}} \quad \text{and} \quad \Delta F_{\mathrm{TOA}} = -(F^{\mathrm{w}}_{\mathrm{TOA}} - F^{\mathrm{o}}_{\mathrm{TOA}}), \tag{1}$$

respectively, where F^{w} and F^{o} are the net fluxes with and without aerosols, respectively. With this convention, a negative sign of the daily ΔF implies an aerosol cooling effect. The profiles of AOT were obtained by integrating the lidar-derived extinction coefficient profiles from the ground up to a given altitude. The profiles of SSA and of the asymmetry factor were obtained by stratifying the atmosphere (PBL + dust on J22, PBL + smoke on J23 and only PBL on J24) according to the lidar profiles' stratification and assigning the sun-photometer-derived values obtained on each day. The asymmetry factor and the surface albedo used as input in GAME were obtained from AERONET level 2 products.

In order to check the suitability of GAME to estimate correctly the downward solar fluxes at the surface, simulated values of GAME are compared to those measured by the pyranometer (figure 4(a)) for clear sky days only in the period 20–31 July. Despite the small number of points the agreement is rather good, with a normalized bias of +5.05% and a root mean square (RMS) of 44 W m^{-2}.

The direct SW radiative forcing calculations (instantaneous values) are summarized in table 2. The positive forcing at TOA on J22 is remarkable since it reflects the strong absorbing effect of the mineral dust discussed earlier. In our case, dust aerosols heat the 'earth–atmosphere' system. One can note the large instantaneous surface forcing with a negative value of −93 W m^{-2}, which is in the range of amplitude proposed by Meloni *et al* (2003). The association of the cooling effect at the surface together with heating of the atmosphere could significantly impact the air quality over Barcelona, following the interaction between aerosols, radiations and local meteorology (impact of the aerosol forcing on the PBL height, dispersion of pollutants) as proposed by Péré *et al* (2011) among others.

For smoke aerosols, the direct forcing at TOA on J23 is in contrast negative, which indicates that among the two characteristics of the smoke plume (low SSA and low asymmetry factor) the scattering aspect predominates at TOA. However, we can observe large differences (table table 2) between BOA (−73 W m^{-2}) and TOA (−13 W m^{-2}) forcing, indicating that a significant part of the solar energy is caped within the atmospheric layer where smoke aerosols are located, heating it (see the following part). At the surface, our estimation of SW forcing is consistent with two of the few references proposed over the Mediterranean by Cachorro *et al* (2008) and Formenti *et al* (2002), with −78 W m^{-2} (instantaneous calculations) and −64 W m^{-2} (daily).

Figure 4(b) represents the instantaneous aerosol SW heating rate, HER. The SW HER decreases sharply around 1 km in all three cases. On J22 the mineral dust considerably increases the SW HER in the lofted layer up to 2.2 K day^{-1}. On J23 the smoke plume has the same effect on the SW HER, which reaches 2.7 K day^{-1}. These values are consistent with former studies (Mallet *et al* 2008).

5. Summary

An intense Saharan dust outbreak and an extremely fresh smoke plume (<5 h) were observed over Barcelona on 22–23 July 2009. Dust and smoke layers were observed between 1–6 and 1–4 km, with associated AE$^{\alpha}$ of 0.4–0.5 and 2.0 and lidar ratios at 532 nm of 51 and 36 sr, respectively. From a preliminary analysis the relatively low SSA of dust (0.83 $\pm$ 0.04) compared to smoke (0.86 $\pm$ 0.04) particles at 440 nm could be due to a mixing of dust with polluted and smoke aerosols. In those conditions the dust particles produced a positive instantaneous SW radiative forcing at TOA of +8 W m^{-2} at 12 UT, while the smoke produced a negative forcing of −13 W m^{-2} at 17 UT. In terms of energy budget, the enhanced absorption of the mixing of dust with polluted and smoke aerosols made the dust behave like a greenhouse gas by heating the 'earth–atmosphere' system, while the very fresh smoke did not behave very differently from fresh or aged smoke.

Acknowledgments

This work is supported by the 7th Framework Programme project Aerosols, Clouds, and Trace Gases Research Infrastructure Network (ACTRIS) (grant agreement no. 262254); by the Spanish Ministry of Science and Innovation and FEDER funds under the projects TEC2009-09106/TEC and CGL2011-13580-E/CLI; and the Spanish Ministry of Education, Culture and Sport for the 'Salvador de Madariaga' project PR2011-0358. The authors gratefully acknowledge the Earth Sciences Division of the Barcelona Supercomputing Center for the use of the Barcelona AERONET sun-photometer data, and the NOAA Air Resources Laboratory (ARL) for the provision of the HYSPLIT transport and dispersion model and READY website (www.arl.noaa.gov/ready.html).

References

Alados-Arboledas L, Müller D, Guerrero-Rascado J L, Navas-Guzmán F, Pérez-Ramírez D and Olmo F J 2011 Optical and microphysical properties of fresh biomass burning aerosol retrieved by Raman lidar, and star-and sun-photometry *Geophys. Res. Lett.* **38** L01807

Ansmann A, Riebesell M and Weitkamp C 1990 Measurement of atmospheric aerosol extinction profiles with a Raman lidar *Opt. Lett.* **15** 746–8

Burton S P, Ferrare R A, Hostetler C A, Hair J W, Rogers R R, Obland C F, Butler M D, Cook A L, Harper D B and Froyd K D 2012 Aerosol classification using airborne High Spectral Resolution Lidar measurements—methodology and examples *Atmos. Meas. Technol.* **5** 73–98

Cachorro V E, Toledano C, Prats N, Sorribas M, Mogo S, Berjón A, Torres B, Rodrigo R, de la Rosa J and De Frutos A M 2008 The strongest desert dust intrusion mixed with smoke over the Iberian Peninsula registered with Sun photometry *J. Geophys. Res.* **113** D14S04

Dubovik O, Holben B, Eck T F, Smirnov A, Kaufman Y J, King M D, Tanré D and Slutsker I 2002 Variability of absorption and optical properties of key aerosol types observed in worldwide locations *J. Atmos. Sci.* **59** 590–608

Dubuisson P, Buriez J C and Fouquart Y 1996 High spectral resolution solar radiative transfer in absorbing and scattering media: application to the satellite simulation *J. Quant. Spectrosc. Radiat. Transfer* **55** 103–26

EEA (European Environment Agency: Joint Public Hearing) 2006 Natural disasters—how should Europe respond? (www.eea.europa.eu/pressroom/speeches/20-03-2006)

Fernald F G 1984 Analysis of atmospheric lidar observations: some comments *Appl. Opt.* **23** 652–3

Formenti P *et al* 2002 STAAARTE-MED 1998 summer airborne measurements over the Aegean Sea. 2. Aerosol scattering and absorption, and radiative calculations *J. Geophys. Res.* **107** 4451–64

Giorgi F and Lionello P 2008 Climate change projections for the Mediterranean region *Glob. Planet. Change* **63** 90–104

Holben B *et al* 1998 AERONET—a federated instrument network and data archive for aerosol characterization *Remote Sens. Environ.* **66** 1–16

Jorba O *et al* 2011 The DAURE field campaign: meteorological overview *Atmos. Chem. Phys. Discuss.* **11** 4953–5001

Klett J D 1985 Lidar inversion with variable backscatter/extinction ratios *Appl. Opt.* **24** 1638–43

Mallet M *et al* 2008 Aerosol direct radiative forcing over Djougou (northern Benin) during the African Monsoon Multidisciplinary Analysis dry season experiment (Special Observation Period-0) *J. Geophys. Res.* **113** D00C01

Meloni D, di Sarra A, DeLuisi J, Di Iorio T, Fiocco G, Junkermann W and Pace G 2003 Tropospheric aerosols in the Mediterranean: 2. Radiative effects through model simulations and measurements *J. Geophys. Res.* **108** 4317–32

Meloni D, di Sarra A, Pace G and Monteleone F 2006 Aerosol optical properties at Lampedusa (Central Mediterranean): 2. Determination of single scattering albedo at two wavelengths for different aerosol types *Atmos. Chem. Phys.* **6** 715–27

Péré J C, Mallet M, Pont V and Bessagnet B 2011 Impact of aerosol direct radiative forcing on the radiative budget, surface heat fluxes, and atmospheric dynamics during the heat wave of summer 2003 over western Europe: a modeling study *J. Geophys. Res.* **116** D23119

Sasano Y and Nakane H 1984 Significance of the extinction/backscatter ratio and the boundary value term in the solution for the two-component lidar equation *Appl. Opt.* **23** 11–3

Sicard M, Rocadenbosch F, Reba M N M, Comerón A, Tomás S, García-Vízcaino D, Batet O, Barrios R, Kumar D and Baldasano J M 2011 Seasonal variability of aerosol optical properties observed by means of a Raman lidar at an EARLINET site over Northeastern Spain *Atmos. Chem. Phys.* **12** 3115–30

Van Drooge B L, Lopez J F and Grimalt J O 2012 Influences of natural emission sources (wildfires and Saharan dust) on the urban organic aerosol in Barcelona (Western Mediterranean Basis) during a PM event *Environ. Sci. Pollut. Res.* at press (doi:10.1007/s11356-012-0890-4)